Electronic Supplementary Material (ESI) for Chemical Science.

Electronic Supplementary Material (ESI)

Visualizing partial solvation at the air-water interface

K. D. Judd, S. W. Parsons, D. B. Eremin, V. V. Fokin, and J. M. Dawlaty*

Department of Chemistry, The University of Southern California, Los Angeles, CA 90089, USA

Corresponding author: J. M. Dawlaty

E-mail: dawlaty@usc.edu

Content:

S1. Experimental Section

Materials. All chemicals were used as received. 1-azido-2-eicosanol (AzEOH), 1-azido-2-hexanol (AzEOH), and eicosylammonium chloride (ENH_3^+) were synthesized. All other chemicals were commercially bought. Their purity, commercial source, and abbreviations as applicable are given as follows: sodium eicosylsulphate (ESO_4^-, Santa Cruz Biotechnology, ≥ 99%), eicosanol (EOH, Sigma, 98%), NaCl (Thermo Scientific, ≥ 99.5%), NaOH (Sigma, ≥ 99.99%), HCl (Sigma, ACS Grade), chloroform (Macron, ACS Grade), methanol (VWR, HPLC Grade), dimethyl sulfoxide (DMSO, Sigma, ACS Grade), tetrahydofuran (THF, Sigma, ACS Grade), ethyl acetate (Sigma, ACS Grade), anisole (Acros Organics, 99%), toluene (Sigma, ≥ 99.9%), acetone (VWR, HPLC Grade), 2-propanol (Sigma, HPLC Grade). trifluoro ethanol (Sigma, ≥ 99%), cyclohexane (Sigma, HPLC Grade), and water (Sigma, HPLC Grade).

Sample Preparation. 2.5 μmol/ml solutions of all pure surfactants were prepared in chloroform, with the exception of ESO_4^- which was prepared in a 50:50 mixture of chloroform and methanol. Mixed surfactant solutions were prepared by dilution of AzEOH solution with EOH, ESO_4^-, or ENH_3^+ solutions.

Surface Pressure-Area (Π-A) Isotherms. Π-A isotherms were measured using a Langmuir trough (KSV Nima, KN1003) equipped with delrin barriers. The volume of the trough was 125 mL with an uncompressed surface area of 243 cm^2. The surface tension was measured using a filter paper Wilhelmy plate connected to a Langmuir balance calibrated to 72.5 mN/m using HPLC water. Surface pressure (Π) is the surface tension when the monolayer is present (γ_M) subtracted from the surface tension without the monolayer (γ_0):

$$\Pi = \gamma_0 - \gamma_M \quad (1)$$

Surfactant monolayers were formed by spreading 25 μL of the pure or mixed surfactant solution onto the surface of the aqueous solution in the trough. This resulted in a mean molecular area (MMA) of 65 Å^2/molecule before barrier compression. After 5 minutes to allow for spreading solvent evaporation the barriers were compressed continuously at 10 mm/min until the monolayer collapsed. All Π-A isotherms shown are the average of 3 trials.

Infrared Reflectance-Absorbance Spectroscopy (IRRAS). Monolayers were held at 30 mN/m throughout IRRAS data collection. A Nicolet iS50 FT-IR was used as the unpolarized IR source. The IRRAS setup was similar to those reported previously.[1–3] After passing through a 500 mm focal length CaF_2 lens the IR light was directed by a gold mirror to the Langmuir trough at an angle of 44° with respect to the surface normal. An identical gold mirror directed the IR light through another CaF_2 focusing lens to a liquid nitrogen cooled MCT detector (Infrared Associates, Model MCT-13-1.0-SL12). For every condition reported 12 spectra were recorded using 128 scans and a resolution of 4 cm^{-1}. First, a background spectrum was recorded by reflection from the aqueous surface of the Langmuir trough without a monolayer. Next, the surfactant solution was added, and the monolayer was compressed to 30 mN/m and 3 consecutive spectra were recorded. After cleaning the Langmuir trough with HPLC water, this process was repeated 2 more times resulting in 9 trials from 3 different monolayers along with 3 background spectra. The *negative* of the reflectance-absorbance (RA) spectrum for each trial was calculated to make the peak of interest positive:

$$-RA = log\left(\frac{R}{R_0}\right) \quad (2)$$

Where R is one of the 9 IR spectra with a monolayer present and R_0 is the average of all 3 background spectra collected for that condition. All spectra shown in this work are the average of these 9 RA trials after a blind spline baseline fit using 10-12 points on each side of the peak but allowing the fit to determine the baseline beneath the peak. Reported peak area is the integrated area beneath the entire peak from 2070 – 2170 cm^{-1}, and the frequency reported is the frequency with the largest intensity (mode) after the above processing and additional 10-point Savitsky-Golay smoothing filter. These properties were determined for all 9 trials per condition, and the reported data points and error are the average and standard deviation of these 9 trials.

Transmission FTIR. HDOHAz solutions were prepared at either 10 or 50 mM. Vibrational spectra were collected using the same Nicolet iS50 FT-IR as described above in single-beam transmission configuration. The pure solvent and AzHOH solutions were placed between two CaF_2 windows to obtain the background and sample spectra, respectively. A DTGS detector with a 400-4000 cm^{-1} range was used, and all settings were the same as described for the reflection experiments. The background and sample were transformed into absorbance and the frequency was determined as described for IRRAS experiments above.

NMR. ^{1}H and ^{13}C{^{1}H} NMR spectra were acquired on Varian 400MR instruments at 400.1 MHz frequency for proton channel. All chemical shifts (δ) are provided in ppm and all coupling constants (*J*) are expressed in Hz. ^{1}H NMR spectra were referenced using residual protic solvent as an internal reference δ 7.26 ppm for $CHCl_3$ in $CDCl_3$; δ 3.31 ppm for methanol-d_3 in methanol-d_4. ^{13}C{^{1}H } NMR spectra were referenced to the solvent peak δ 77.16 ppm for $CDCl_3$ or δ 49.0 ppm for methanol-d_4. The spectra were processed using MestReNova v14.2.3 software package.

GC-qToF-MS. The GC-MS measurements were performed with an Agilent 7890 GC system equipped with an Agilent 7250 qToF mass detector (electron ionization, 70 eV and 15 eV for low-EV mode to obtain molecular ion) and an HP-5MS column (30 m × 0.25 mm × 0.25 µm film) using He as a carrier gas at a flow of 2.0 mL × min^{-1}. The following temperature program was used in the GC-MS measurements: initial temperature: 60 °C, hold for 1 min, then 30 °C × min^{-1} to 300 °C and hold for 3 min. Nitrogen was used as a collision gas. All the GC-MS spectra were recorded at 1 Hz. The spectra were extracted using the Agilent MassHunter 10.0 software package, then the spectra were converted to txt format and post-processed using the software written in Python using the NumPy and Pandas packages. Spectra were processed by pyOpenMS package. Mass spectra and chromatograms were plotted using the Matplotlib package.

LC-ESI–(+)MS experiments. Mass spectra were measured using an Agilent 6545XT qToF instrument coupled with 1290 LC system. The qToF mass spectrometer was equipped with an ESI ionization source. In positive ion mode ionization parameters are as follows: Capillary Voltage –4.0 kV, Nozzle Voltage 0 V, nitrogen was applied as a nebulizer gas 35 psi, dry gas 12 L × min^{-1}, 300 °C, sheath gas 12 L × min^{-1}, 275 °C and collision gas. Spectra were recorded in *m/z* 50 –

900 range. The following LC solvent gradient was used at 0.4 mL × min^{-1} flow rate: A – 0.1% FA in H_2O, B – 0.1% FA in MeOH; hold 30% B for 1 min, ramp 30% to 85% B in 5 min, and hold B for 4 min; 4 min postrun time for column re-equilibration. All the LC-MS spectra were recorded at 4 Hz. The spectra were extracted using the Agilent MassHunter 10.0 software package, then the spectra were converted to txt format and post-processed using the software written in Python using the NumPy and Pandas packages. Spectra were processed by pyOpenMS package. Mass spectra and chromatograms were plotted using the Matplotlib package.

ATR-FT-IR. The FT-IR measurements were performed with an Agilent Cary 630 instrument. The azide characterization data was acquired with diamond ATR sampling using pure materials directly with no sample preparation. The spectra were converted to csv format and post-processed using the software written in Python using the NumPy and Pandas packages. The spectra were plotted using the Matplotlib package.

Synthesis of 1-azido-2-eicosanol (AzEOH)

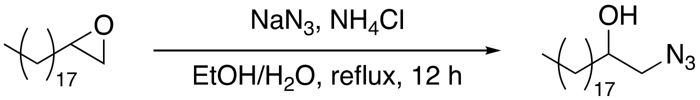

A 1-neck round bottom flask (250 mL) with a magnetic stirring bar was charged with 1,2-epoxyeicosane (10 mmol, 2.96 g) and dissolved in EtOH (18 mL) and H_2O (4.5 mL). Ammonium chloride (13 mmol, 0.70 g) and sodium azide (13 mmol, 0.85 g) were added consequently while mixture was extensively stirring to avoid lumps of solid formation. Mixture was stirred for 12 h at reflux, then cooled down to r.t., and product was extracted with 3×50 mL DCM. Combined organic fraction was washed with 3×50 ml of water and 2×50 ml of brine, dried over $MgSO_4$, and filtered. Solvent was removed under reduced pressure and product was redissolved in minimal amount of hexanes. Solution was passed through 2 cm thick pad of silica, washed with 50 mL of hexanes, then eluted with 1:10 EtOAc:hexanes. Eluent was removed under reduced pressure and product was recrystallized from hot hexanes (10 mL per 1 g of material) at 50 °C cooling to r.t. Double recrystallization and drying under reduced pressure afford >99% purity white flaky crystalline product containing a single 2-hydroxy isomer.

Purity was confirmed by GC-MS and NMR.

Yield (white flaky crystalline solid) 1.89 g; 56% (yield of doubly recrystallized product).

^1H NMR (399.7 MHz, $CDCl_3$; δ, ppm): 3.76 (s, 1H), 3.38 (dd, J = 12.4, 3.4 Hz, 1H), 3.25 (dd, J = 12.4, 7.4 Hz, 1H), 1.87 (s, 1H), 1.52 – 1.42 (m, 3H), 1.25 (br s, 31H), 0.88 (t, J = 6.7 Hz, 3H).

$^{13}C\{^1H\}$ NMR (100.5 MHz, $CDCl_3$; δ, ppm): 71.0, 57.3, 34.5, 32.1, 29.85, 29.84, 29.81, 29.79, 29.71, 29.67, 29.66, 29.52, 25.6, 22.9, 14.3. (five signals are lost due to resolution)

GC-MS(TOF): exact for $C_{20}H_{41}NO$ $[M - N_2]^{+\bullet}$ *m/z* 311.3182, accurate *m/z* 311.3178 (Δ = 1.5 ppm).

ATR-IR (selected bands, cm^{-1}): 2119 (ν, N=N=N), 2848 (ν_s, CH_2), 2914 (ν_{as}, CH_2).

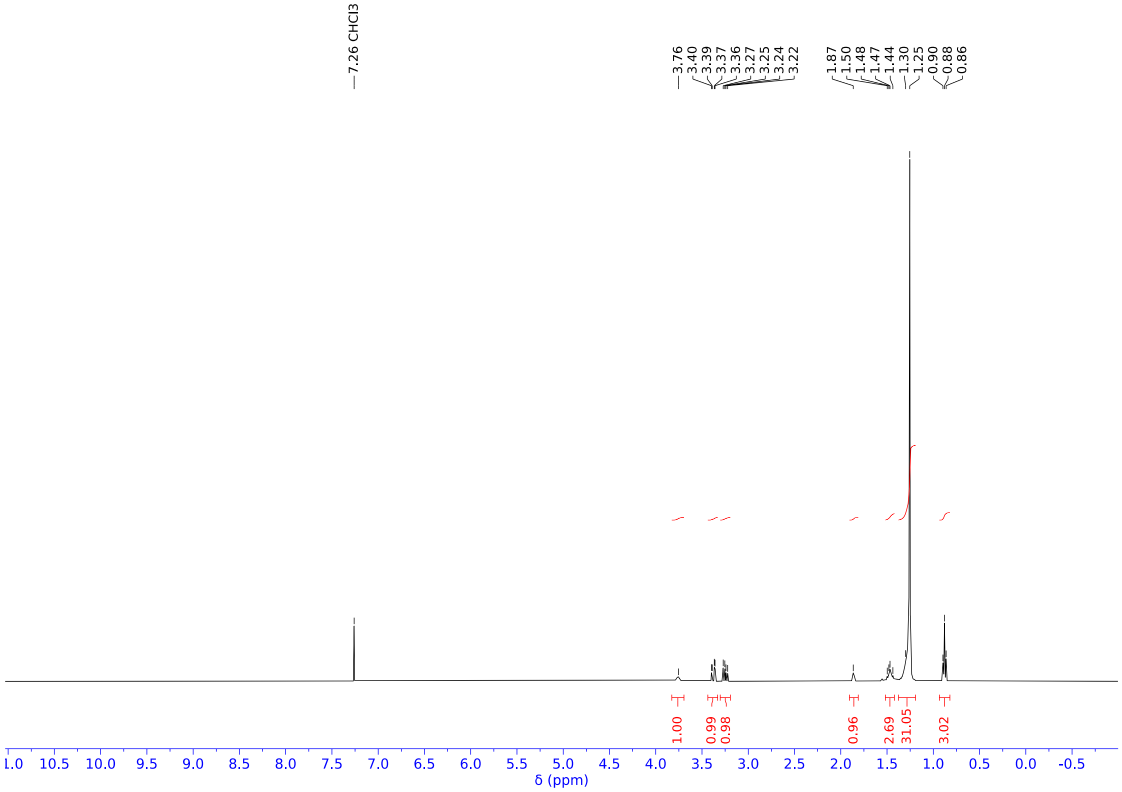

Fig. S1 ^{1}H NMR spectrum of 1-azido-2-eicosanol in $CDCl_3$.

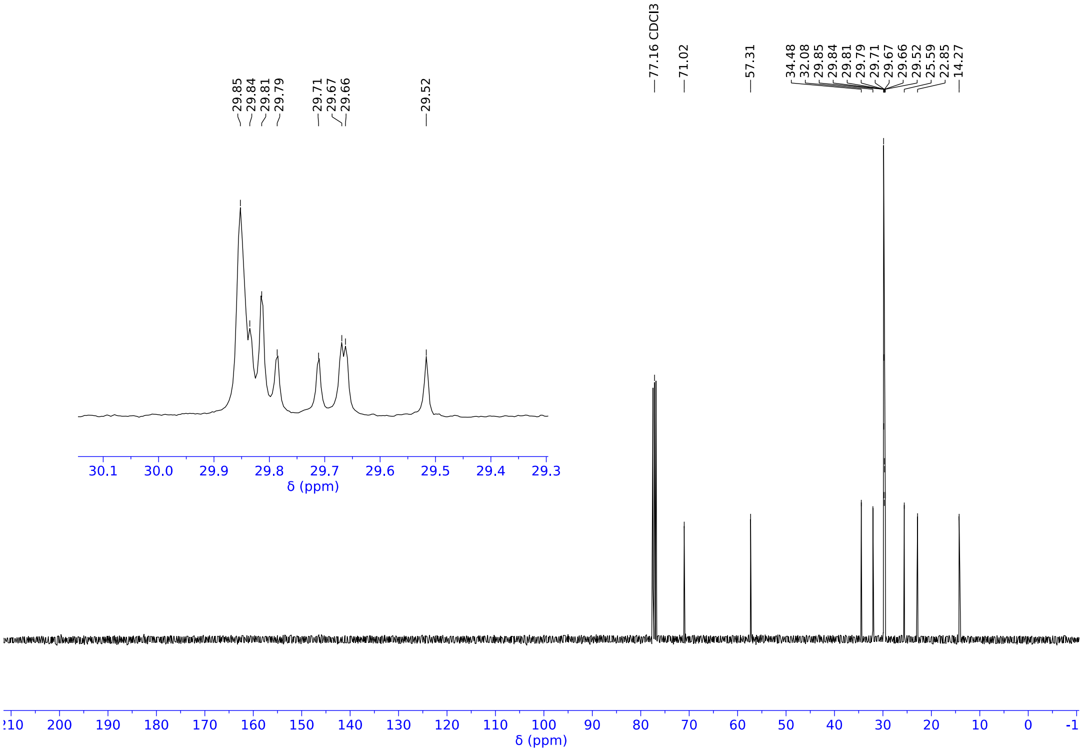

Fig. S2 ^{13}C NMR spectrum of 1-azido-2-eicosanol in $CDCl_3$.

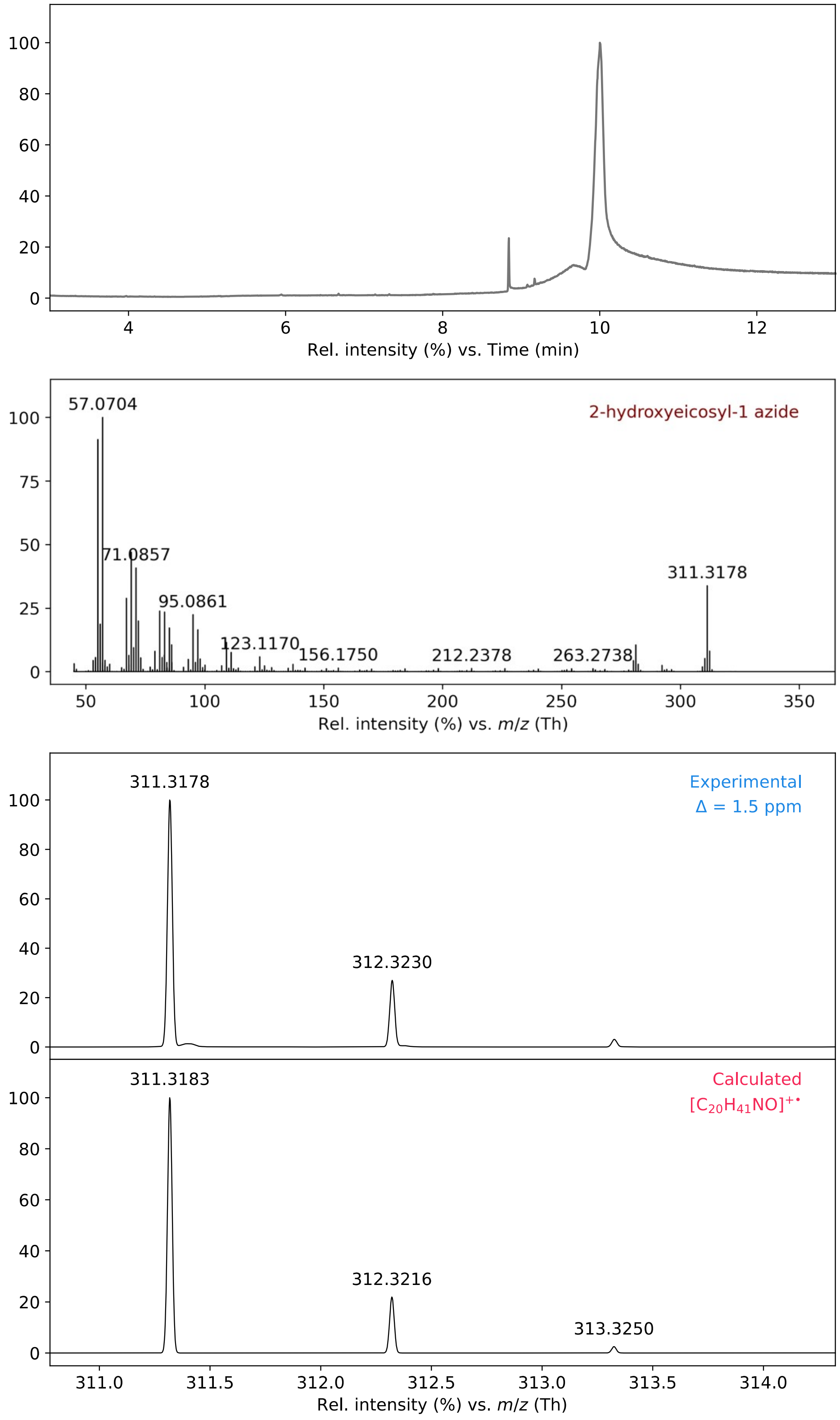

Fig. S3 GC-EI-MS(TOF) analysis of 1-azido-2-eicosanol (top) chromatogram, (middle) mass spectrum extracted from GC-MS peak, (bottom) experimental and calculated spectra for $[M - N_2]^{+\bullet}$ ion.

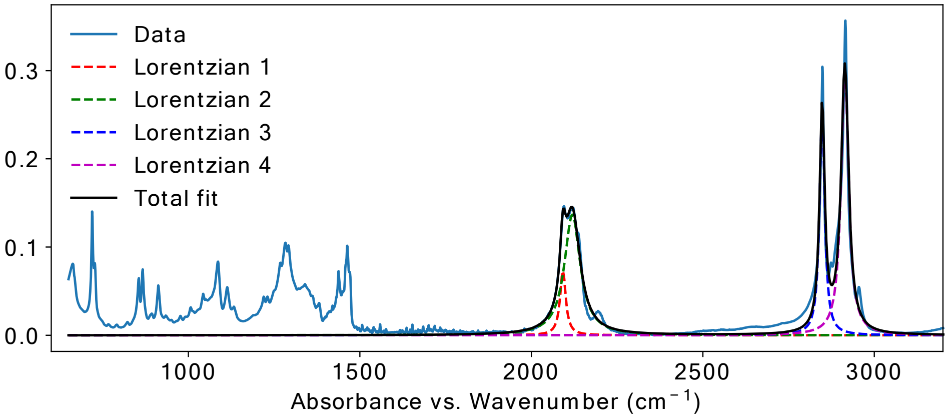

Fig. S4 ATR-IR spectrum of pure 1-azido-2-eicosanol.

Synthesis of 1-azido-2-hexanol (AzHOH)

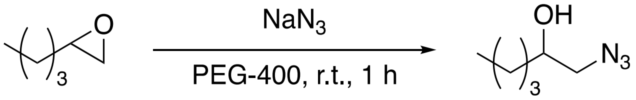

A 1-neck round bottom flask (100 mL) with a magnetic stirring bar was charged with 1,2-epoxyhexane (10 mmol, 1.00 g) and dissolved in PEG-400 (20 g). Sodium azide (12 mmol, 0.78 g) were added while mixture was stirring. Mixture was stirred for 6 h at r.t., then poured onto H_2O (50 mL) and was extracted with 3×30 mL of EtOAc. The solvent was removed and the crude product was redissolved in 1 mL of hexanes and solution was passed through 2 cm thick pad of silica, washed with 20 mL of hexanes, then eluted with 1:10 EtOAc:hexanes. Eluent was removed under reduced pressure to afford pure product as colourless liquid.

Yield (colourless liquid) 0.49 g; 35%.

^{1}H NMR (399.7 MHz, $CDCl_3$; δ, ppm): 3.80 – 3.72 (m, 1H), 3.38 (dd, J = 12.4, 3.4 Hz, 1H), 3.25 (dd, J = 12.4, 7.4 Hz, 1H), 1.91 (s, 1H), 1.56 – 1.24 (m, 6H), 0.91 (t, J = 7.0 Hz, 3H).

^{13}C{^{1}H} NMR (100.5 MHz, $CDCl_3$; δ, ppm): 71.0, 57.3, 34.2, 27.7, 22.7, 14.1.

GC-MS(TOF): exact for $C_5H_{11}O$ $[M - CH_2N_3]^+$ *m/z* 87.0804, accurate *m/z* 87.0806 (Δ = 1.6 ppm).

ATR-IR (selected bands, cm^{-1}): 2095 (ν, N=N=N).

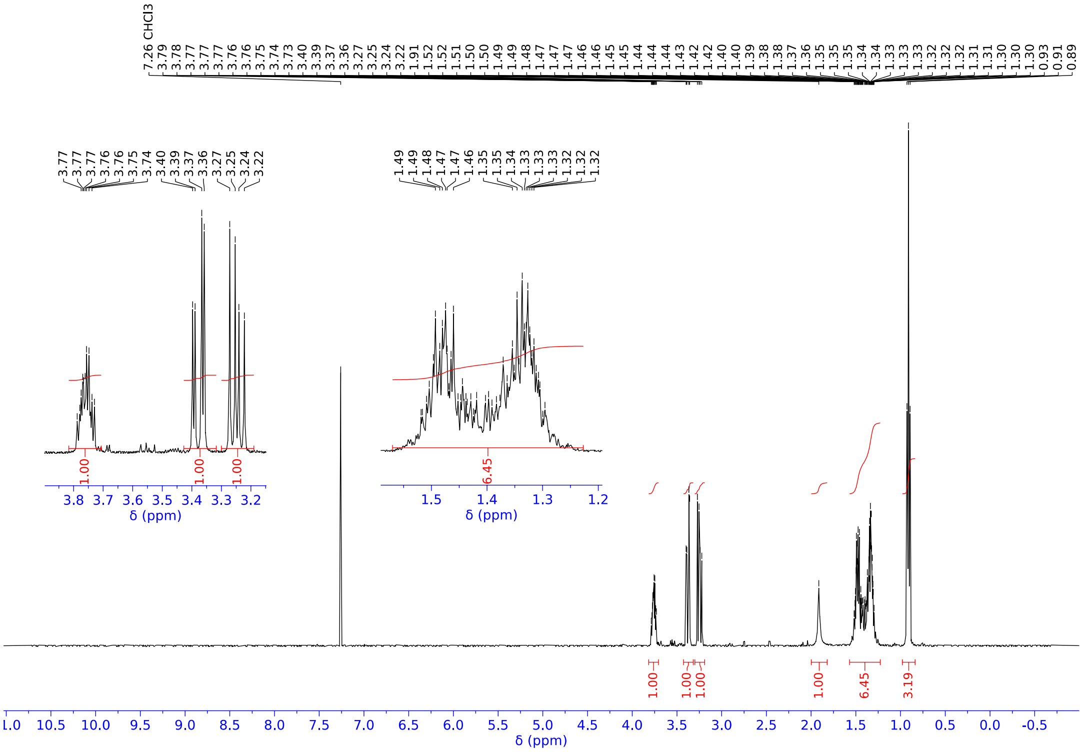

Fig. S5 ^{1}H NMR spectrum of 1-azido-2-hexanol in $CDCl_3$.

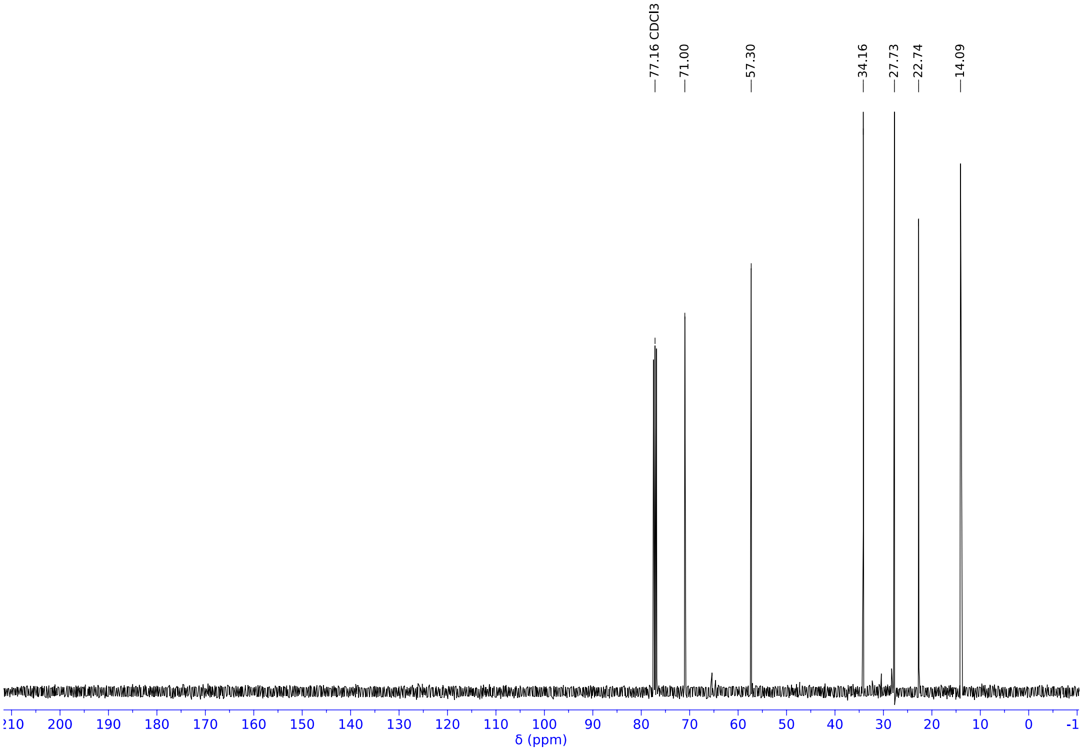

Fig. S6 ^{13}C NMR spectrum of 1-azido-2-hexanol in $CDCl_3$.

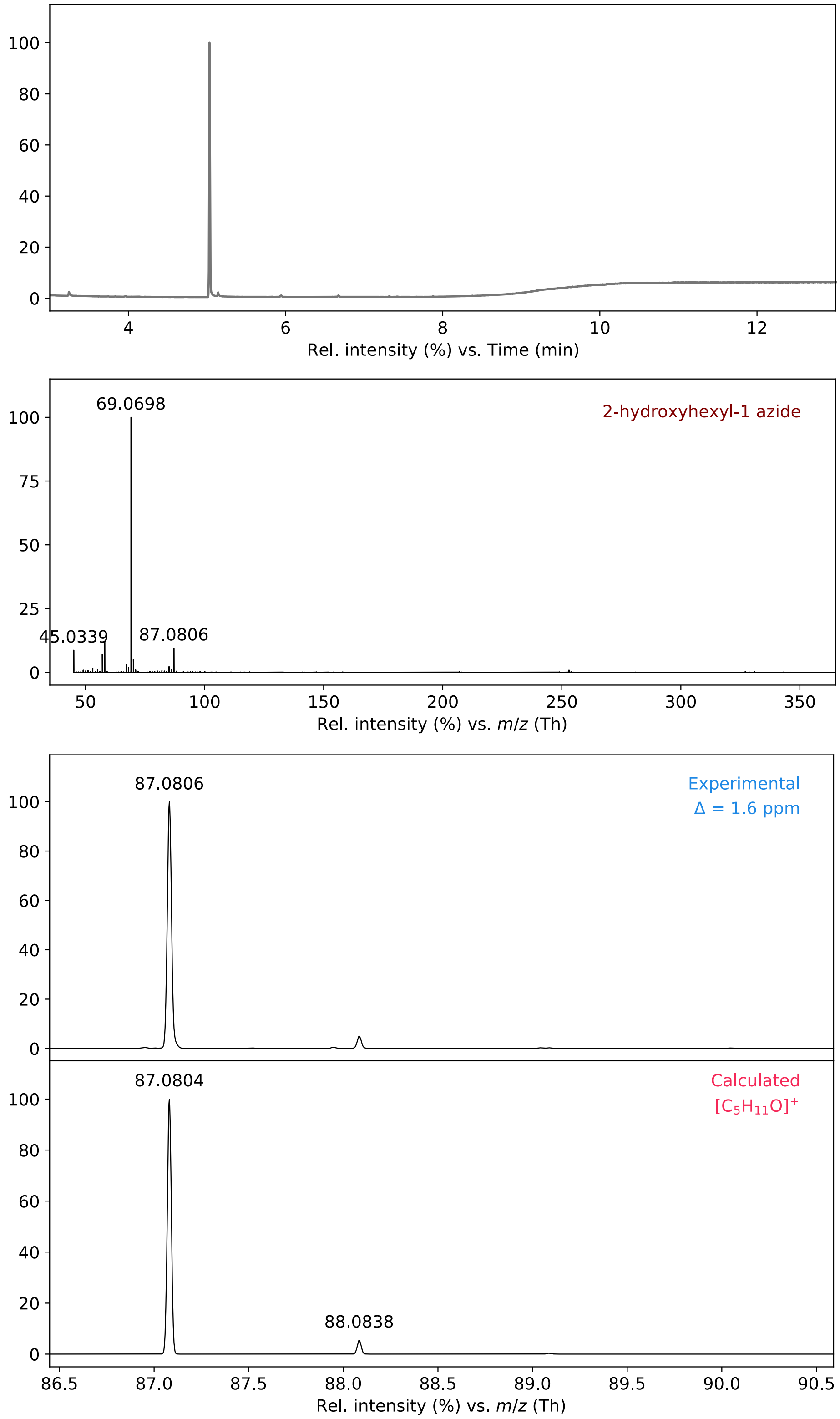

Fig. S7 GC-EI-MS(TOF) analysis of 1-azido-2-hexanol (top) chromatogram, (middle) mass spectrum extracted from GC-MS peak, (bottom) experimental and calculated spectra for $[M - CH_2N_3]^+$ ion.

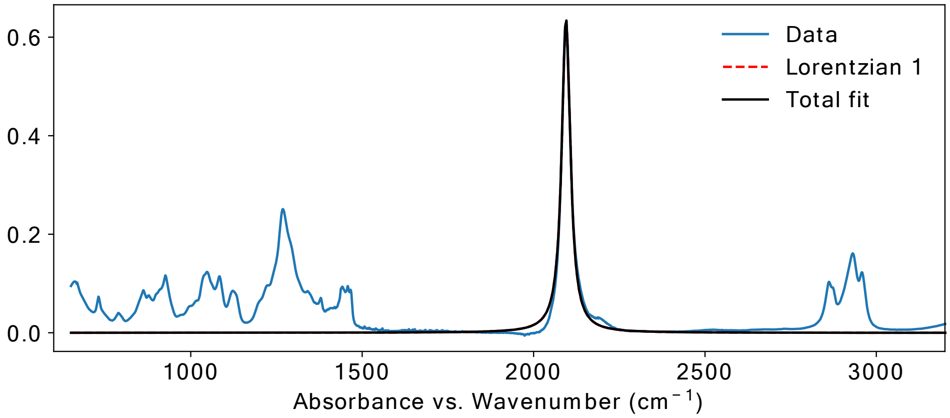

Fig. S8 ATR-IR spectrum of 1-azido-2-hexanol.

Synthesis of 1-eicosyl azide

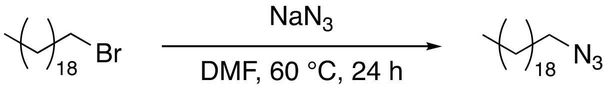

A 1-neck round bottom flask (250 mL) with a magnetic stirring bar was charged with 1-eicosyl bromide (13.8 mmol, 5 g) and dissolved in DMF (75 ml). Sodium azide (20.7 mmol, 1.35 g) was added while mixture was extensively stirring to avoid lumps of solid formation. Mixture was stirred for 24 h at 60 °C, then 50 mL of water were added, and product was extracted with 3×50 mL Et_2O. Combined organic fraction was washed with 3×50 ml of water and 2×50 ml of brine, dried over Na_2SO_4 with C_{act} and passed through a short pad of silica. Pure product was obtained after solvent removal under reduced pressure. Purity was confirmed by GC-MS and NMR.

Yield (white which turns yellow after 2 h crystalline solid) 4.34 g; 97%.

^{1}H NMR (399.7 MHz, $CDCl_3$; δ, ppm): 3.25 (t, *J* = 7.0 Hz, 2H), 1.60 (q, *J* = 7.0 Hz, 2H), 1.25 (br s, 35H), 0.88 (t, *J* = 6.7 Hz, 3H).

$^{13}C\{^{1}H\}$ NMR (100.5 MHz, $CDCl_3$; δ, ppm): 51.6, 32.1, 29.85, 29.83, 29.82, 29.78, 29.70, 29.64, 29.52, 29.31, 28.99, 26.9, 22.9, 14.3. (six signals are lost due to resolution)

GC-MS(TOF): exact for $C_{20}H_{41}N$ $[M - N_2]^+$ *m/z* 295.3234, accurate *m/z* 295.3228 (Δ = 1.8 ppm).

ATR-IR (selected bands, cm^{-1}): 2095 (ν, N=N=N), 2849 (ν_s, CH_2), 2915 (ν_{as}, CH_2).

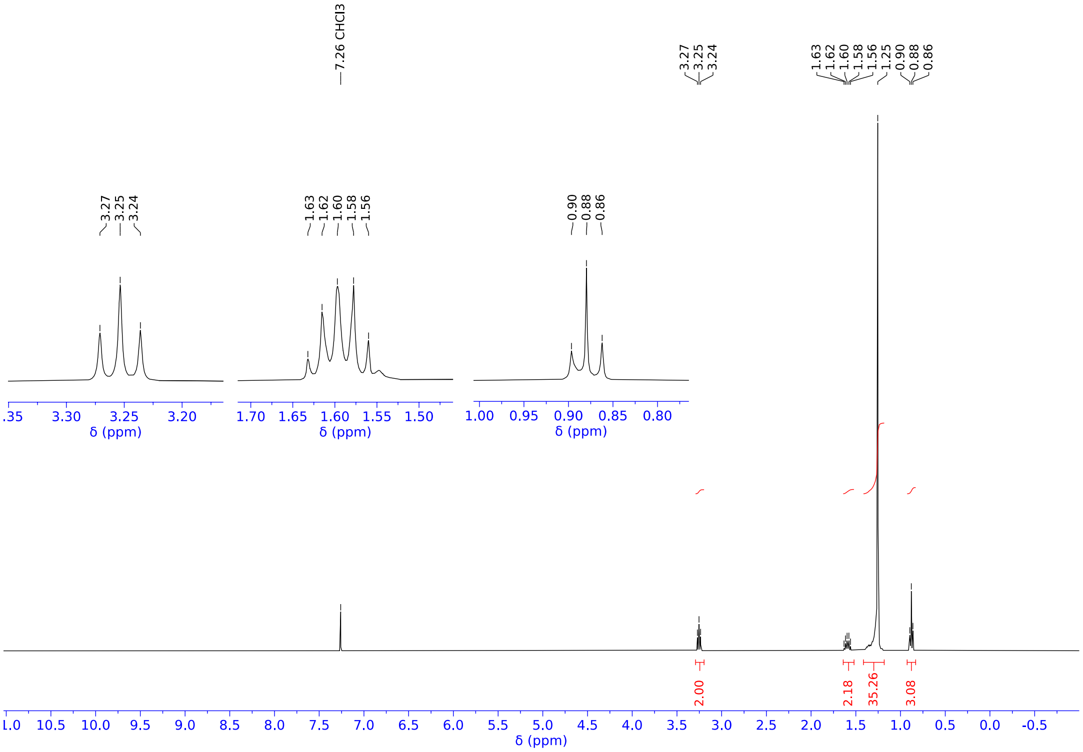

Fig. S9 ^{1}H NMR spectrum of eicosyl azide in CDCl$_3$.

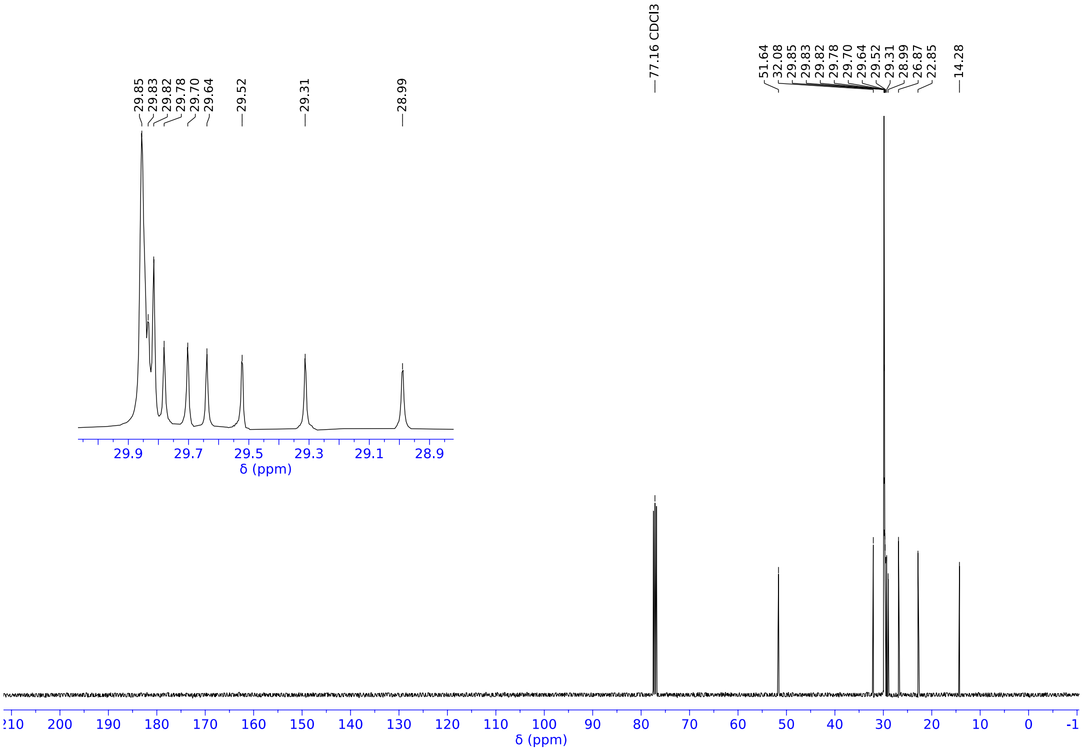

Fig. S10 ^{13}C NMR spectrum of eicosyl azide in CDCl$_3$.

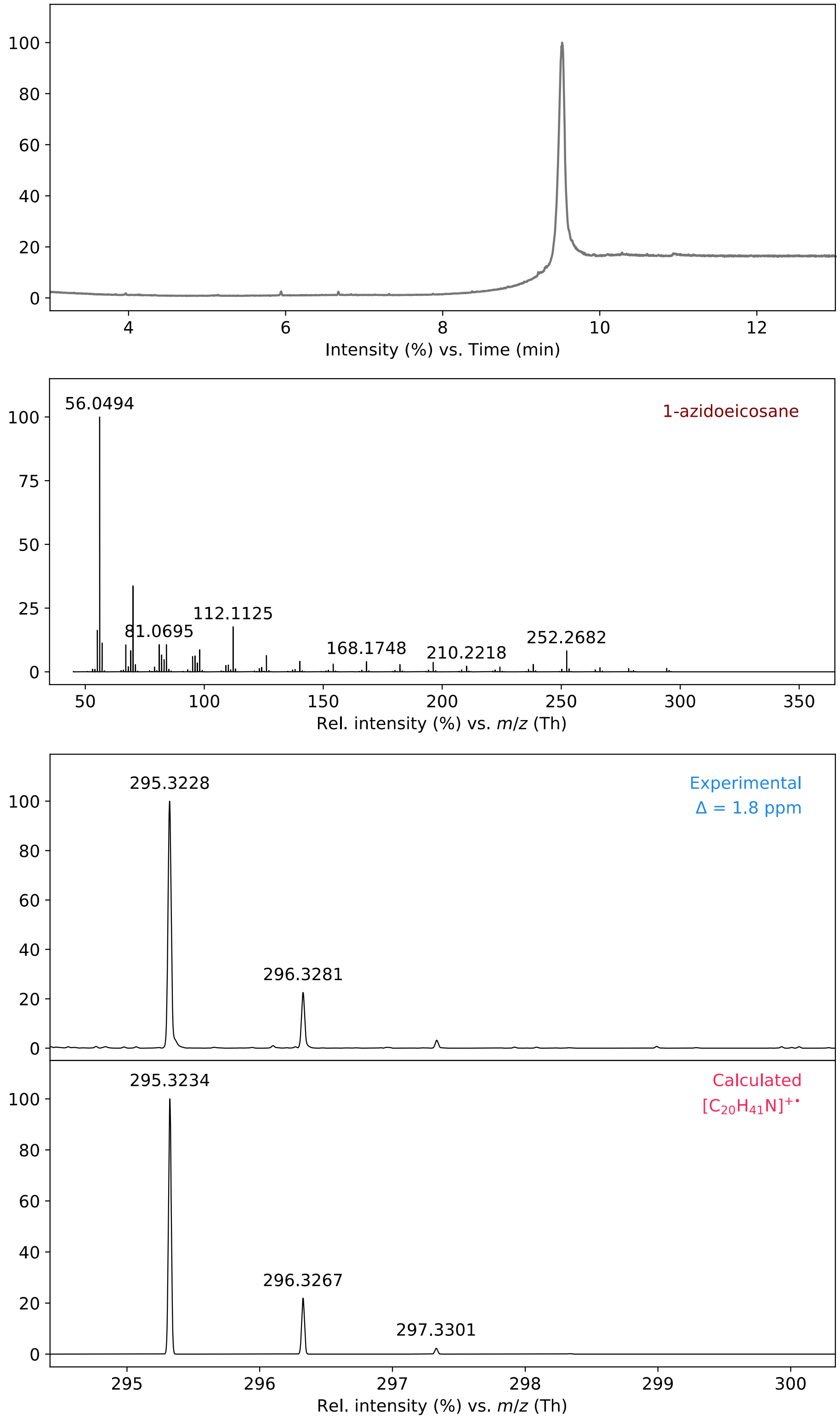

Fig. S11 GC-EI-MS(TOF) analysis of eicosyl azide (top) chromatogram, (middle) mass spectrum extracted from GC-MS peak, (bottom) experimental and calculated spectra for $[M - N_2]^{+\bullet}$ ion.

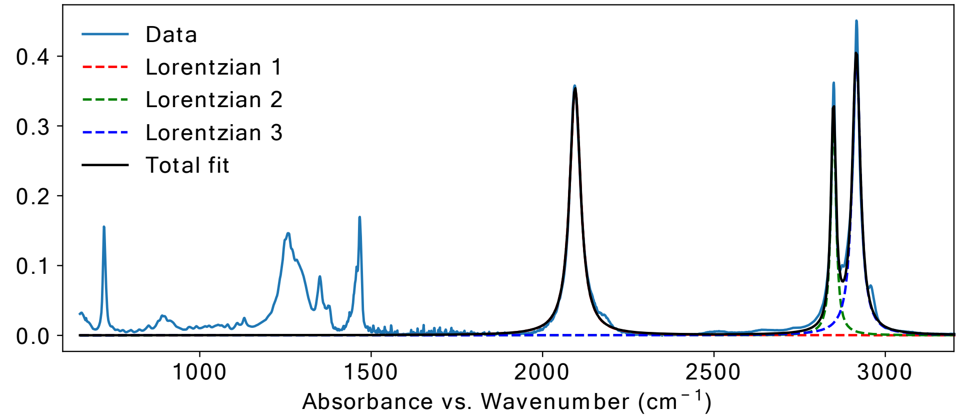

Fig. S12 ATR-IR spectrum of pure eicosyl azide.

Synthesis of 1-aminoeicosane hydrochloride (ENH$_3^+$ chloride)

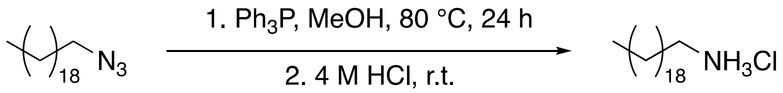

A 1-neck round bottom flask (250 mL) with a magnetic stirring bar was charged with 1-eicosyl azide (13.4 mmol, 4.3 g), MeOH (125 ml), and placed into oil bath set up to 80 °C. Triphenylphosphine (16.1 mmol, 4.22 g) was immediately added while mixture was extensively stirring and flask was equipped with a condenser. Mixture was stirred for 24 h at 80 °C, cooled down to room temperature and concentrated to ca. 25 mL. Slowly 5 mL of 4 M HCl were added. White precipitate formed immediately. The precipitate was filtered, washed with hexanes 3×20 mL, and dried under reduced pressure. Recrystallization from 60 mL of hot MeOH afforded white crystalline product. Purity was confirmed by LC-MS and NMR.

Yield (white crystalline solid) 3.20 g; 72%.

^{1}H NMR (399.7 MHz, CD$_3$OD; δ, ppm): 4.89 (s, 3H), 3.05 – 2.88 (m, 2H), 1.64 (q, *J* = 7.4 Hz, 2H), 1.29 (s, 38H), 0.90 (t, *J* = 6.5 Hz, 3H).

^{13}C{^{1}H} NMR (100.5 MHz, CD$_3$OD; δ, ppm): 40.8, 33.1, 30.79, 30.77, 30.67, 30.53, 30.49, 30.25, 28.6, 27.5, 23.8, 14.5. (eight signals are lost due to resolution)

LC-ESI-MS(TOF): exact for $C_{20}H_{44}N$ $[M – Cl]^+$ *m/z* 298.3468, accurate *m/z* 298.3471 (Δ = 1.0 ppm).

ATR-IR (selected bands, cm^{-1}): 2050 (ν, N-H-Cl), broad, ca. 2887 (ν, N-H), 2848 (ν_s, CH$_2$), 2912 (ν_{as}, CH$_2$).

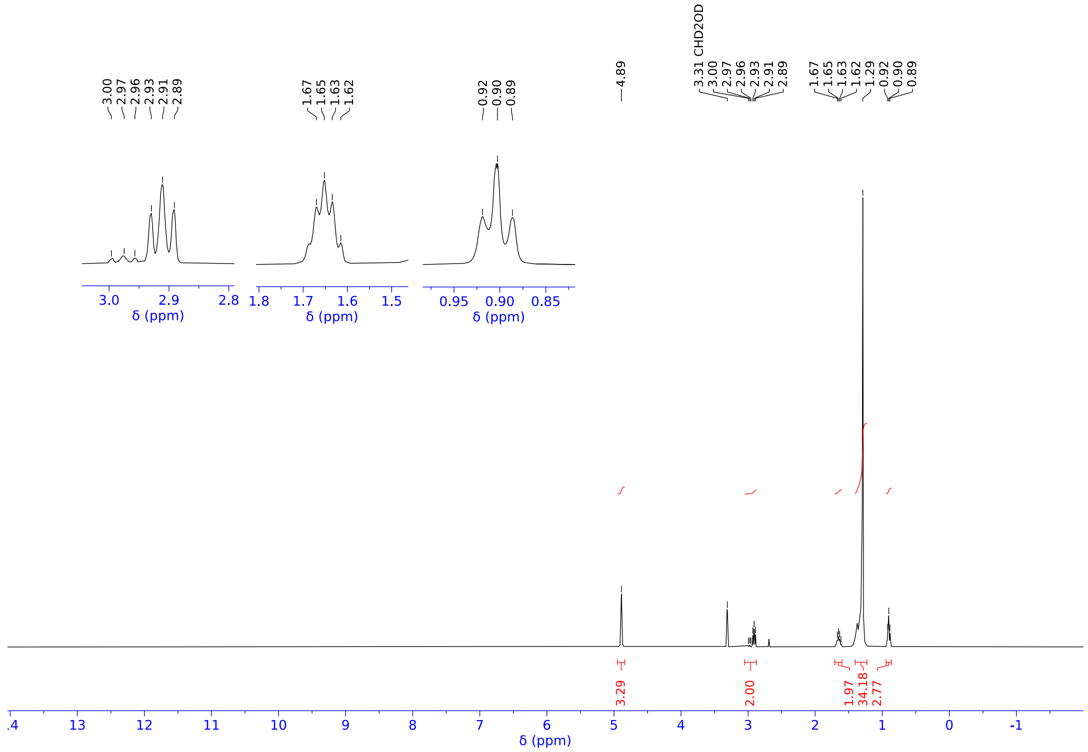

Fig. S13 ^{1}H NMR spectrum of 1-aminoeicosane hydrochloride in CD_3OD.

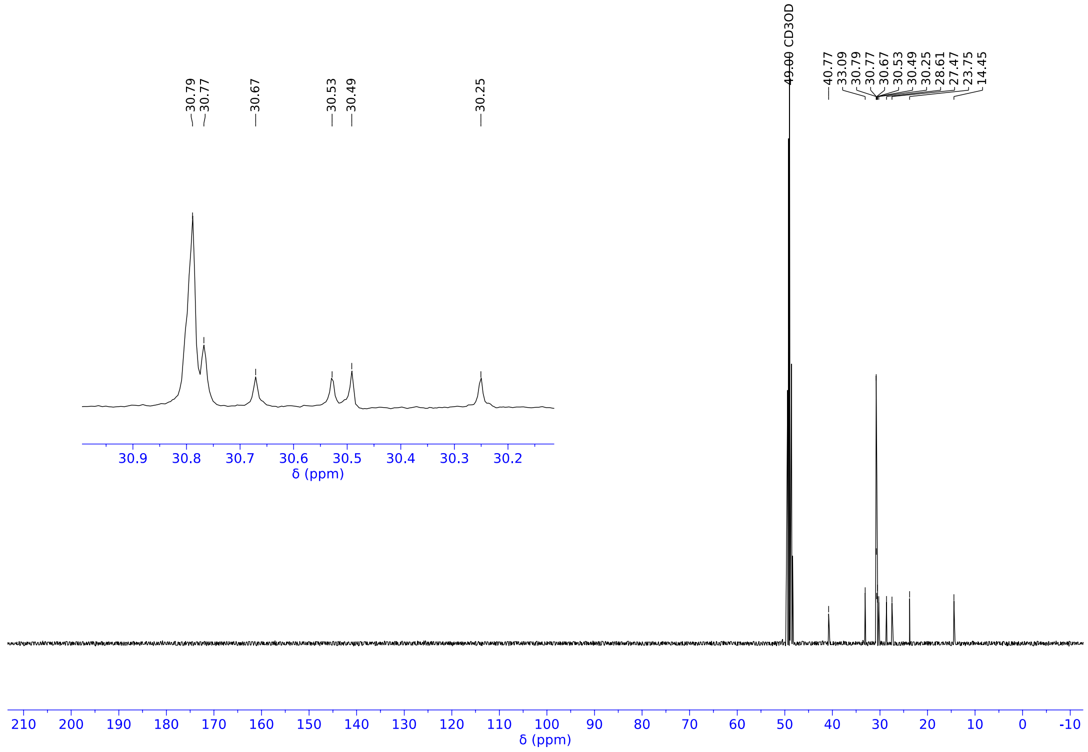

Fig. S14 ^{13}C NMR spectrum of 1-aminoeicosane hydrochloride in CD_3OD.

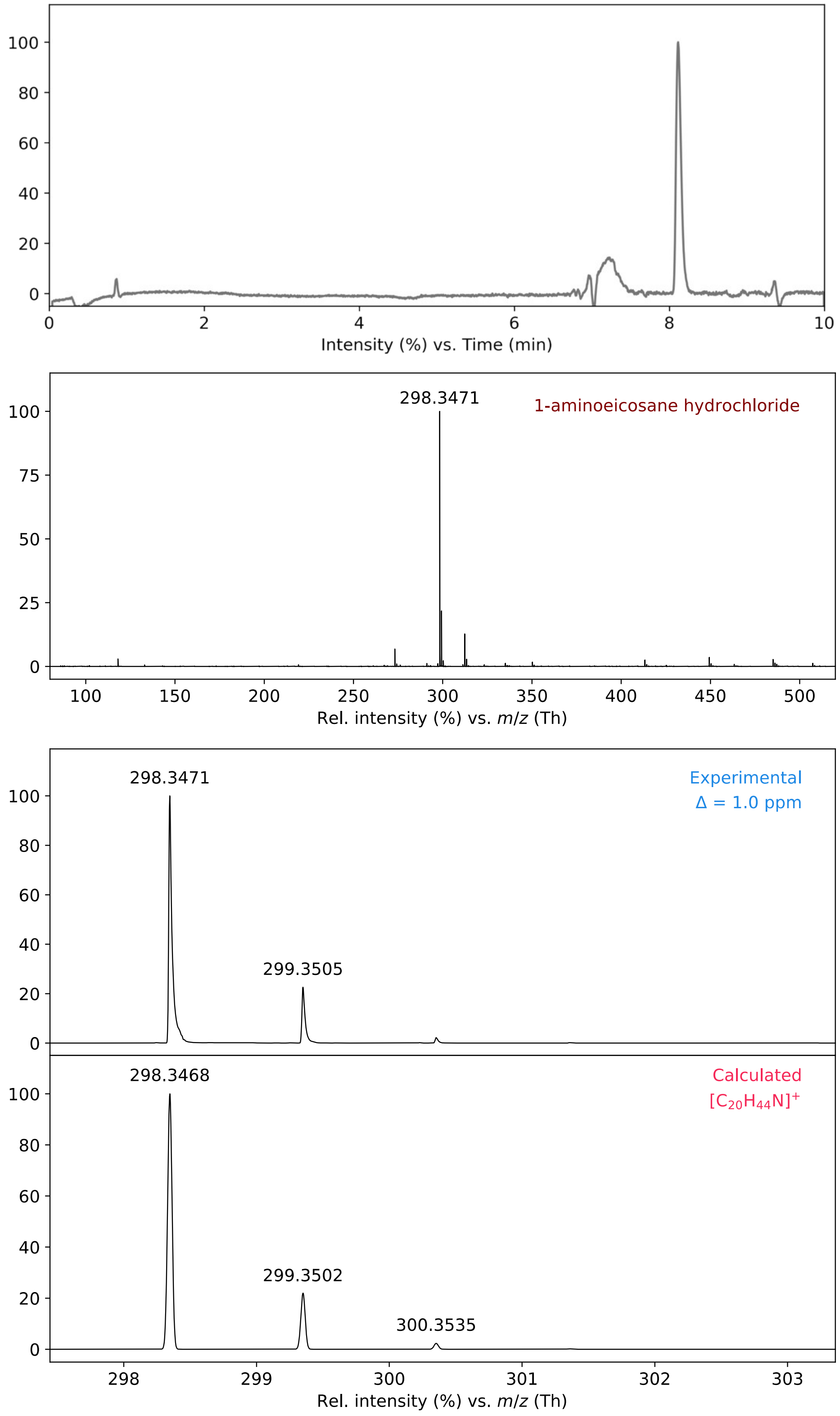

Fig. S15 LC-ESI-MS(TOF) analysis of 1-aminoeicosane hydrochloride (top) chromatogram, (middle) mass spectrum extracted from LC-MS peak, (bottom) experimental and calculated spectra for $[M – Cl]^+$ ion.

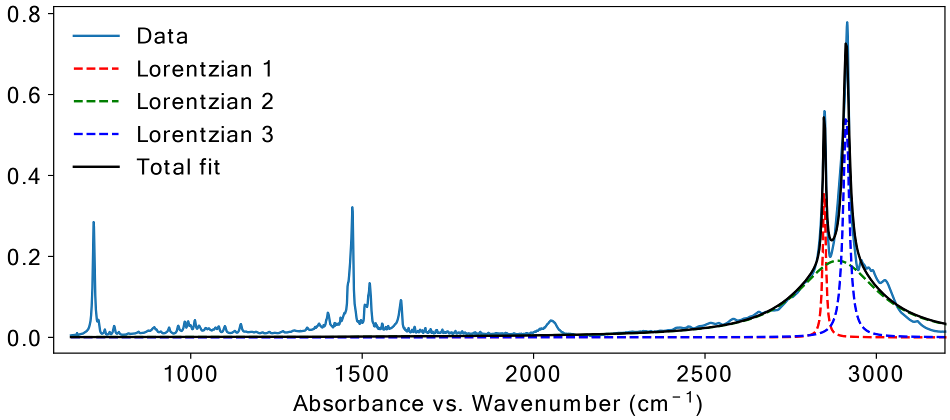

Fig. S16 ATR-IR spectrum of pure 1-aminoeicosane hydrochloride.

S2. Langmuir Trough Isotherms and Surface Charge Density (Fig. 2)

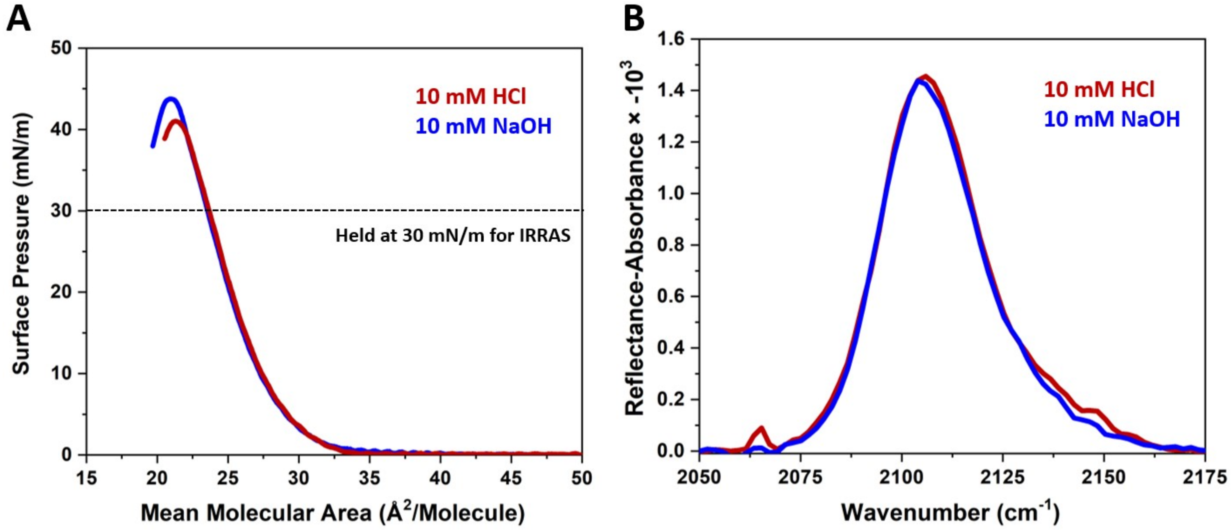

Fig. S17 (**A**) Langmuir trough pressure-area (Π-A) isotherms and (**B**) IRRAS spectra of the azide (N_3) peak of pure AzEOH monolayers held at 30 mN/m. The results over 10 mM HCl (pH 2) and 10 mM NaOH (pH 12) are identical and confirm negligible ion specific effects at this concentration.

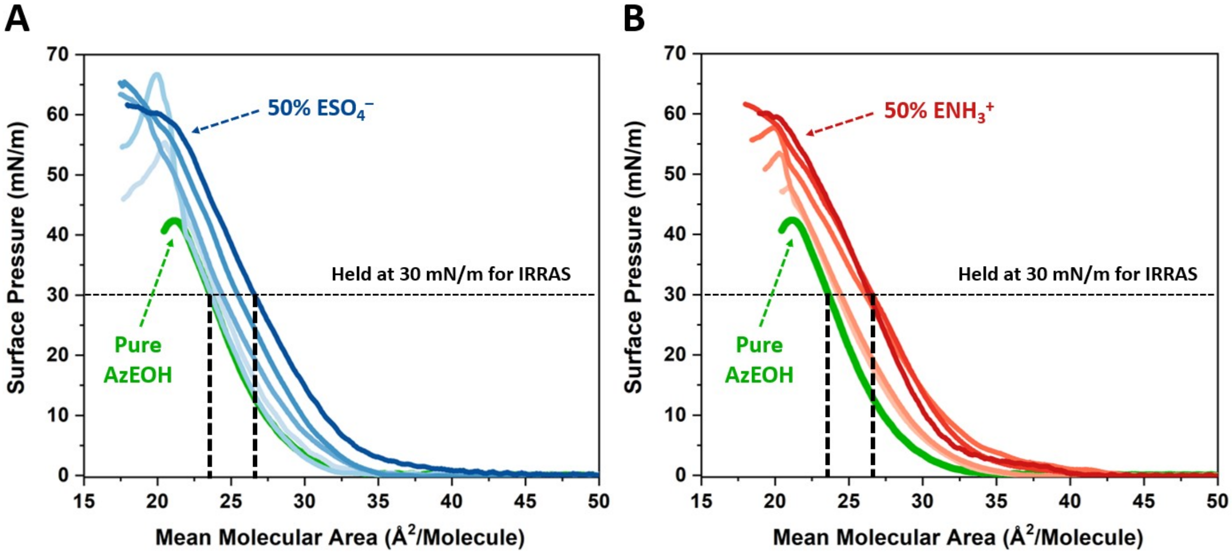

Fig. S18 Π-A isotherms of mixed monolayers of AzEOH with charged (**A**) ESO_4^- or (**B**) ENH_3^+. The mole percentage of charged surfactant ranged from 10% (lighter blue or red) to 50% (darker blue or red) and the averaged HCl/NaOH pure AzEOH isotherm is shown in green. The mean molecular area (MMA) at 30 mN/m was determined graphically from 3 trials per condition. These values are reported in **Table S1** with the calculated azide density and surface charge density (σ).

Table S1 Average MMA, Azide Density, and Surface Charge Density of Mixed Monolayers. Reported values are the average of 3 trials with standard deviation in parentheses.

		@ 30 mN/m Surface Pressure		
Monolayer	Subphase	MMA (Å^2/surfactant)	Azide Density (N_3/nm^2)	Surface Charge Density (e/nm^2)
Pure AzEOH	Combined	23.6 (0.2)	4.23 (0.04)	0 (Reference)
10% ESO_4^-	10 mM NaOH	24.1 (0.4)	3.73 (0.06)	– 0.414 (0.007)
20% ESO_4^-	10 mM NaOH	23.7 (0.6)	3.38 (0.08)	– 0.85 (0.02)
30% ESO_4^-	10 mM NaOH	24.4 (0.1)	2.87 (0.01)	– 1.230 (0.005)
40% ESO_4^-	10 mM NaOH	25.5 (0.1)	2.36 (0.01)	– 1.571 (0.007)
50% ESO_4^-	10 mM NaOH	26.6 (0.1)	1.88 (0.01)	– 1.880 (0.007)
10% ENH_3^+	10 mM HCl	24.4 (0.3)	3.68 (0.05)	+ 0.409 (0.005)
20% ENH_3^+	10 mM HCl	24.4 (0.4)	3.27 (0.06)	+ 0.82 (0.01)
30% ENH_3^+	10 mM HCl	26.1 (0.1)	2.68 (0.01)	+ 1.149 (0.004)
40% ENH_3^+	10 mM HCl	26.7 (0.1)	2.25 (0.01)	+ 1.500 (0.006)
50% ENH_3^+	10 mM HCl	26.4 (0.2)	1.90 (0.02)	+ 1.90 (0.02)

S3. Surface Electrostatics and Acid-Base Equilibria at Charged Surfaces

The goal of this section is to show that based on the standard continuum theory of surface electrostatics for the air-water interface, the interfacial electric field is not significantly affected by the salt concentration at the subphase. Prior to this demonstration, it should be kept in mind that the continuum theories carry several assumptions and approximations that may not hold when considering field variations at the molecular level. Nonetheless, this exercise is useful and provides a coarse picture.

In the continuum electrostatic theory of interfaces charges are modeled as infinitesimally small and the solvent a continuum. The problem is reduced to one dimension *x* starting from the interface and extending into the bulk. The potential profile $\psi(x)$ is retrieved by simultaneously satisfying the Poisson and Boltzmann equations.[1] When a symmetric salt (equal charge for anions and cations) is considered, the potential profile is given by:

$$\psi(x) = \frac{4k_BT}{ze}\text{arctanh}\left[\tanh\left(\frac{ze}{4k_bT}\psi_o\right)e^{-\kappa x}\right] \tag{S3.1}$$

where k_B is the Boltzmann constant, *T* is the temperature, *z* is the charge of an ion, *e* is the fundamental charge, ψ_o is the potential at *x=0*. The characteristic screening length κ is defined as:

$$\kappa = \sqrt{\frac{2nz^2e^2}{\epsilon_r\epsilon_o k_bT}} = \sqrt{\frac{2c_{bulk}z^2F^2}{\epsilon_r\epsilon_o RT}} \tag{S3.2}$$

where *n* is the concentration of the salt, ϵ_r is the dielectric constant, and ϵ_0 is the permittivity of free space. For convenience, the above is also shown in alternate units with c_{bulk} the salt concentration, *F* the Faraday's constant, and *R* the gas constant. In most electrochemical experiments, ψ_o is fixed and dictated by a potentiostat. When the applied potential is small, the profile into the solution is approximately exponential.

$$\psi(x) \approx \psi_o e^{-\kappa x} \tag{S.3.3}$$

The electric field is defined as the negative of the gradient of this potential $E(x) = -\frac{d\psi(x)}{dx}$. At higher salt concentrations, the screening length κ is shorter, which results into steeper decay profiles and larger electric fields.

However, for the air-water interface the potential ψ_o is not dictated externally by a potentiostat, but rather controlled by both surface charge density σ of surfactants and the salt concentration in the bulk c_{bulk}, and given by the Grahame equation.

$$\psi_o = \frac{2k_bT}{ze} * \operatorname{arcsinh}\left[\frac{\sigma}{\sqrt{8RT\epsilon_o\epsilon_r c_{bulk}}}\right] \tag{S.3.4}$$

While high surface charge density σ increases the surface potential ψ_o, high salt concentration partly counteracts that effect and reduces ψ_o. To retrieve the decay profile into the bulk, the above should be inserted into S.3.1. However, note that unlike the electrochemical fixed-potential case, the salt concentration not only affects the decay profile, but also the initial surface potential ψ_o.

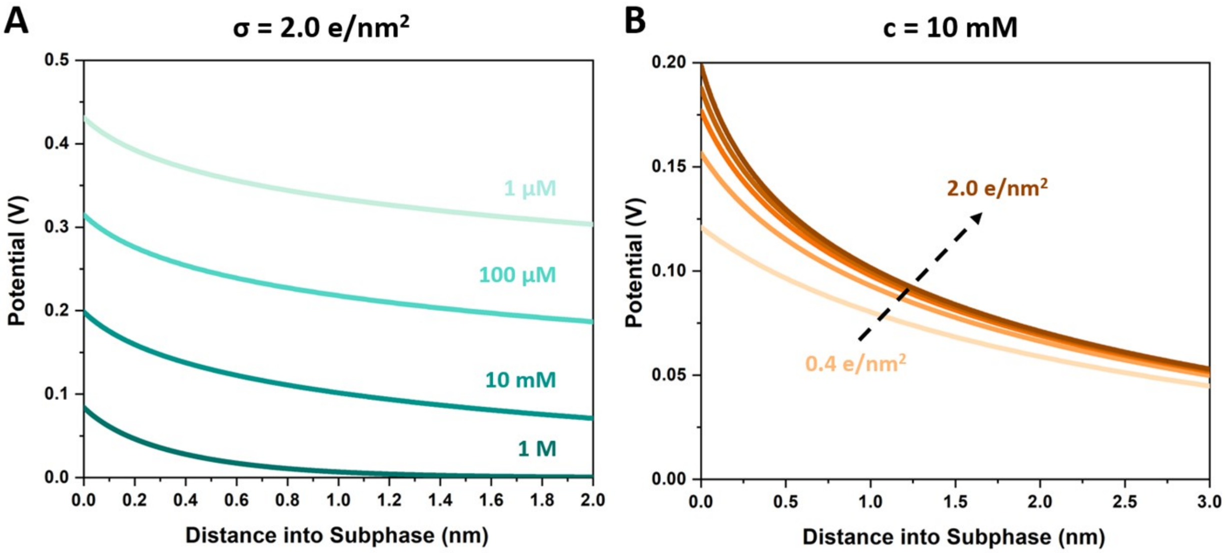

Fig. S19 (**A**) Potential profile as a function of distance into the bulk subphase at constant charge density and several salt concentrations. (**B**) Potential profile for a constant salt concentration and several surface charge densities.

The combination of these effects is such that the electric field $E(x) =- \frac{d\psi(x)}{dx}$ near the surface remains nearly unchanged. We demonstrate this in two ways. First, in Fig. S.3.1.A we plot the potential profile into the bulk for several c_{bulk} all for a fixed surface change density σ. The plots clearly show that higher salt concentrations reduce ψ_o, but the slope of the decay profile remains largely unaltered, even over six orders of magnitude in salt concentration. In contrast, note that altering the surface charge density σ does change both ψ_o and its gradient (Fig. S3.1.B).

Second, we analytically calculate the electric field by differentiating S.3.3.

$$E(x) = \kappa\,\psi_o\,e^{-\kappa x} \tag{S.3.5}$$

which for *x=0* results into $E(0) = \kappa\psi_o$. Replacing ψ_o from S.3.4, expanding the *sinh* function, and keeping up to the linear term results into:

$$E(0) = \sqrt{\frac{8c_{bulk}RT}{\epsilon_r\epsilon_o}}\frac{\sigma}{\sqrt{8RT\epsilon_o\epsilon_r c_{bulk}}} = \frac{\sigma}{\epsilon_o\epsilon_r}$$

which does not have any salt dependence.

S4. Median Frequency and Peak Width Plots (Fig. 5)

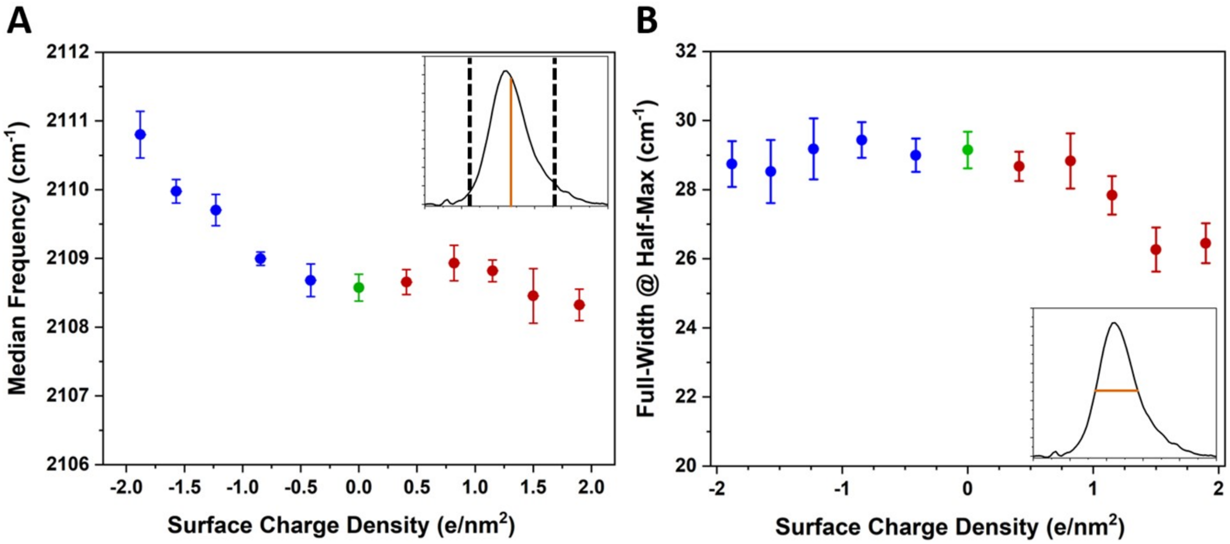

Fig. S20 (**A**) Median frequency and (**B**) full peak width at half maximum intensity (FWHM) of the spectra in **Fig. 3**. The median is determined between 2080 cm^{-1} and 2140 cm^{-1} and is the frequency which splits the peak over this range into equal areas. This frequency is slightly blueshifted relative to the mode frequency reported in **Fig. 5** due to the asymmetry of the peak. The median frequency over the entire peak range (2070 cm^{-1} – 2170 cm^{-1}) shows the same trend with a larger net shift and larger error. These values are reported in tables in **Section S7**.

S5. AzHOH FTIR Spectra/40% Eicosanol Isotherms and Spectra (Fig. 6)

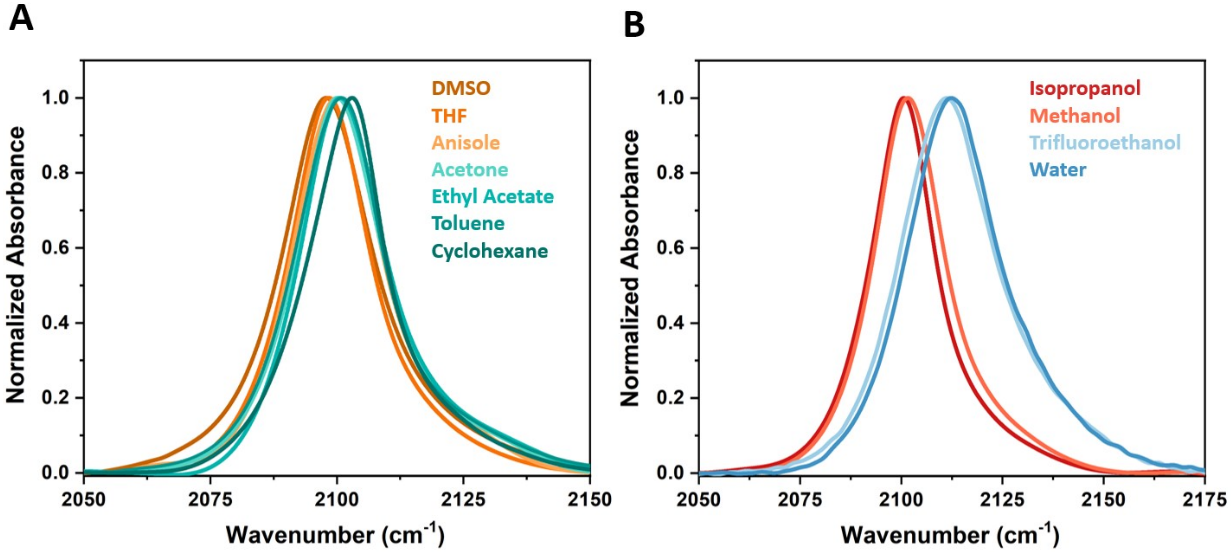

Fig. S21 Spectra for the (**A**) aprotic solvents and (**B**) protic solvents from **Fig. 6** of the main text. The legend entries follow the relative shift order (most red to most blue).

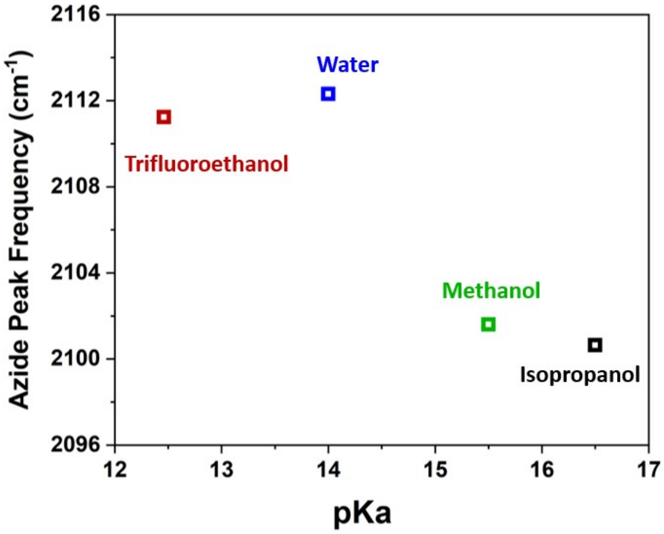

Fig. S22.The peak frequency of the protic solvents plotted against pKa. A similar trend is seen with pKa as with Kamlet-Taft α parameter in **Fig. 6**. pKas obtained taken from Bordwell pKa tables.

Water induces the largest blue shift of the protic solvents despite being a weaker hydrogen bond donor compared to trifluoroethanol, as described by the Kamlet-Taft α parameter. Such behavior has been seen in previous work with similar methylated azides and was attributed to the high H-bonding density in water relative to other solvents.[2]

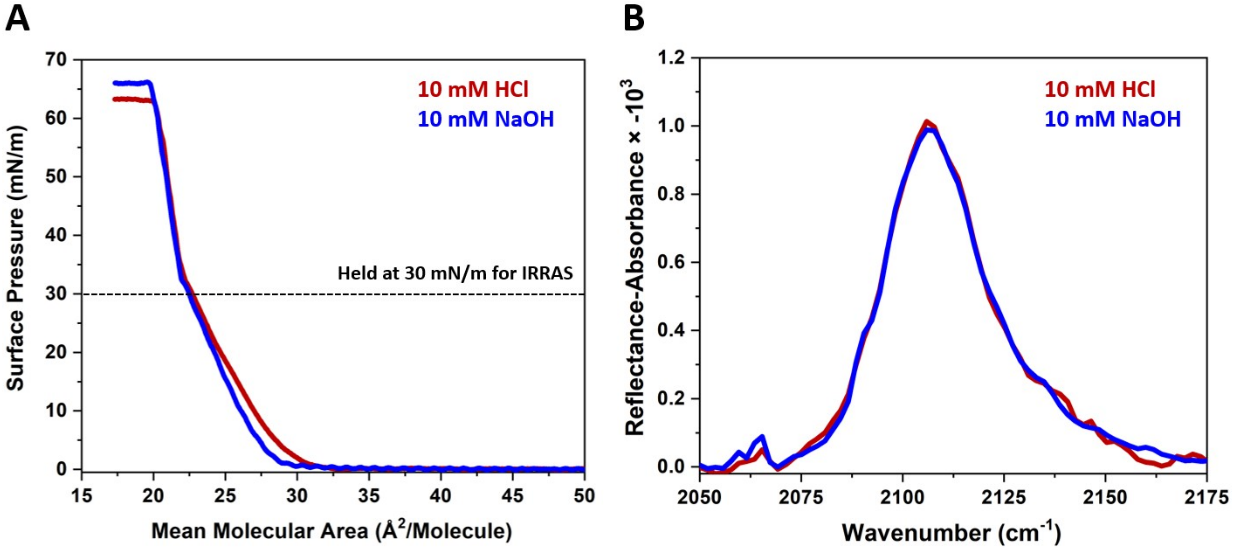

Fig. S23 (**A**) Langmuir trough pressure-area (Π-A) isotherms and (**B**) IRRAS spectra of the azide (N_3) peak of 40% eicosanol monolayers held at 30 mN/m. The results over 10 mM HCl (pH 2) and 10 mM NaOH (pH 12) are identical and confirm negligible ion specific effects at this concentration.

S6. 100 mM and 1000 mM NaCl Isotherms and Spectra (Fig. 7)

Pressure-Area Isotherms

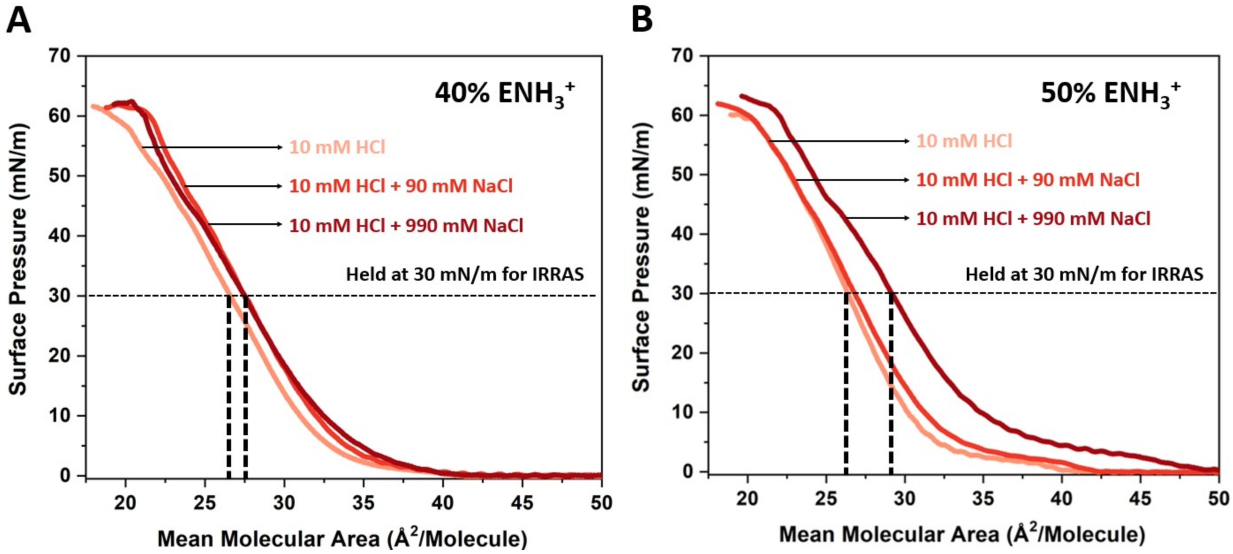

Fig. S24 Π-A isotherms of (A) 40% ENH$_3^+$ and (B) 50% ENH$_3^+$ over subphases with 10 mM HCl and added NaCl. The isotherm over 10 mM HCl alone (**Fig. S18B**) is shown for reference. The mean molecular area (MMA) at 30 mN/m was determined graphically from 3 trials per condition. These values are reported in **Table S2** along with the calculated azide density and surface charge density (σ).

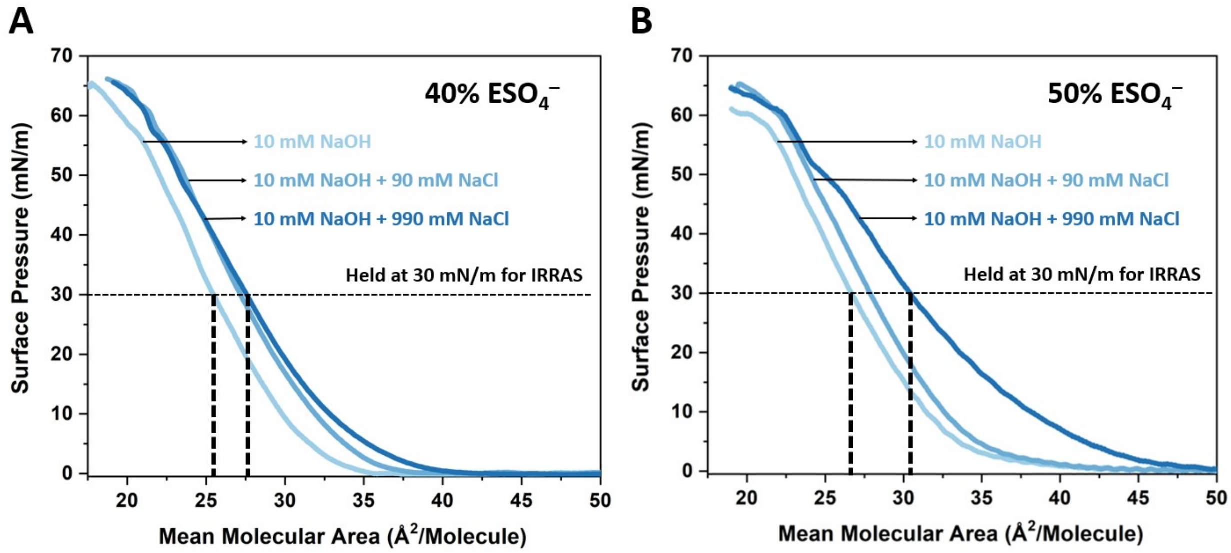

Fig. S25 Π-A isotherms of (A) 40% ESO$_4^-$ and (B) 50% ESO$_4^-$ over subphases with 10 mM NaOH and added NaCl. The isotherm over 10 mM NaOH alone (**Fig. S18A**) is shown for reference. The mean molecular area (MMA) at 30 mN/m was determined graphically from 3 trials per condition. These values are reported in **Table S2** with the calculated azide density and surface charge density (σ).

Table S2. Average MMA, Azide Density, and Surface Charge Density of High Salt Conditions. Reported values are the average of 3 trials with standard deviation in parentheses.

		@ 30 mN/m Surface Pressure		
Monolayer	Added NaCl	Mean Molecular Area (Å^2/surfactant)	Azide Density (N_3/nm^2)	Surface Charge Density (e/nm^2)
40% ESO_4^-	90 mM	27.2 (0.5)	2.21 (0.04)	– 1.47 (0.02)
40% ESO_4^-	990 mM	27.6 (0.5)	2.18 (0.04)	– 1.45 (0.02)
50% ESO_4^-	90 mM	27.9 (0.2)	1.79 (0.01)	– 1.79 (0.01)
50% ESO_4^-	990 mM	31.8 (2.1)	1.6 (0.1)	– 1.6 (0.1)
40% ENH_3^+	90 mM	27.6 (0.3)	2.18 (0.02)	+ 1.45 (0.01)
40% ENH_3^+	990 mM	27.5 (0.3)	2.18 (0.02)	+ 1.46 (0.01)
50% ENH_3^+	90 mM	26.9 (0.3)	1.86 (0.02)	+ 1.86 (0.02)
50% ENH_3^+	990 mM	29.2 (0.1)	1.71 (0.01)	+ 1.712 (0.006)

IRRAS Spectra

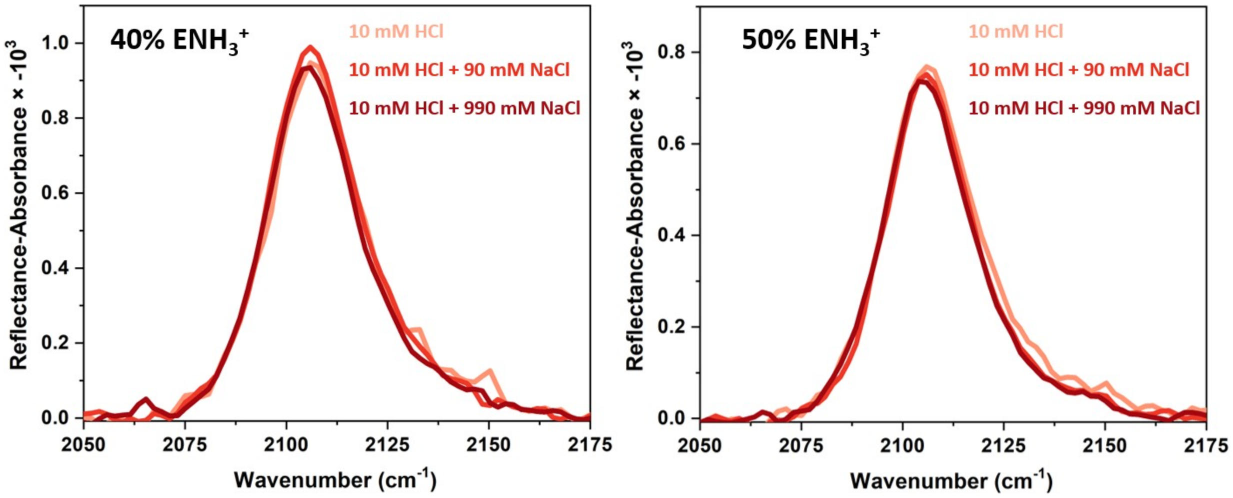

Fig. S26 IRRAS spectra of the azide peak of (A) 40% ENH_3^+ and (B) 50% ENH_3^+ over subphases with 10 mM HCl and added NaCl. The spectrum over 10 mM HCl alone (Main text **Fig. 3**) is shown for reference. All spectra and reported peak properties are averaged from 9 trials.

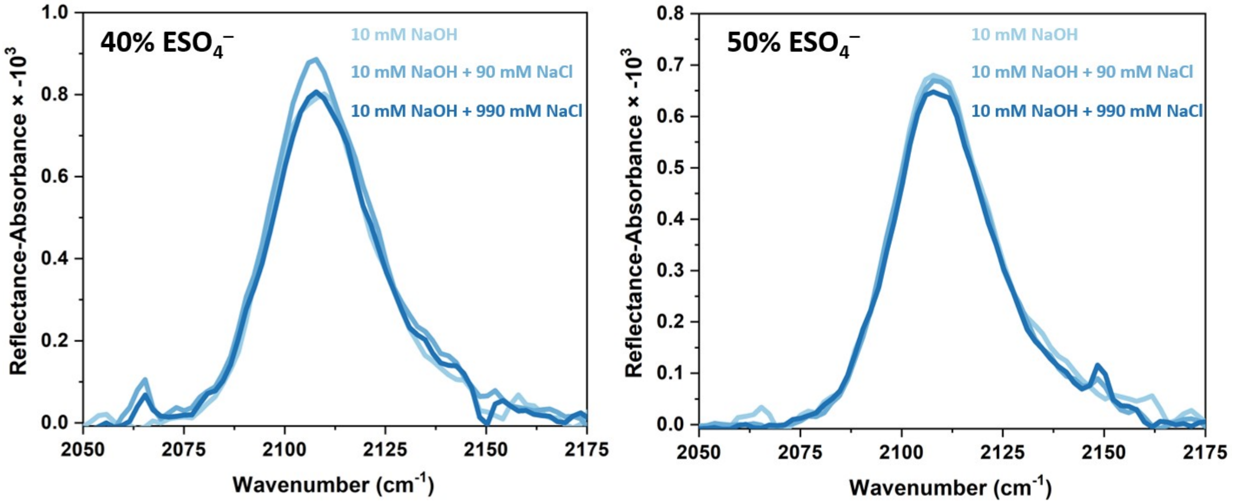

Fig. S27 IRRAS spectra of the azide peak of (**A**) 40% ESO$_4^-$ and (**B**) 50% ESO$_4^-$ over subphases with 10 mM NaOH and added NaCl. The spectrum over 10 mM NaOH alone (Main text **Fig. 3**) is shown for reference. All spectra and reported peak properties are averaged from 9 trials.

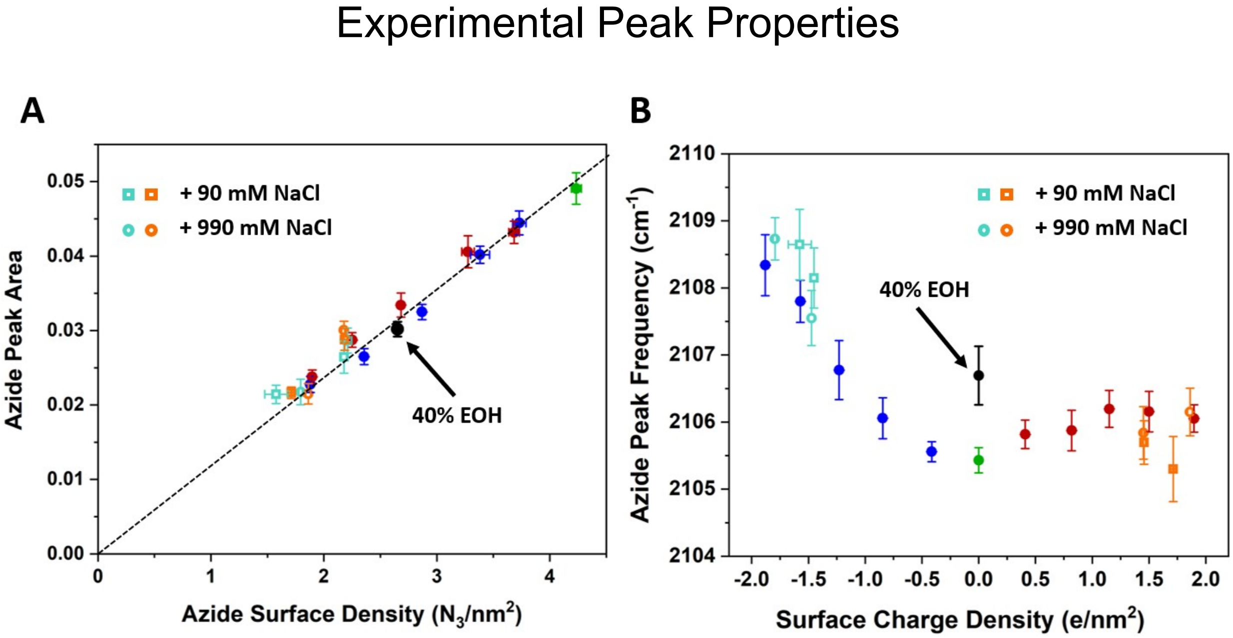

Fig. S28 (**A**) Azide peak area (main text **Fig. 4**) and (**B**) azide frequency (main text **Fig. 5**) including data points with added NaCl to the subphase and 40% EOH monolayers.

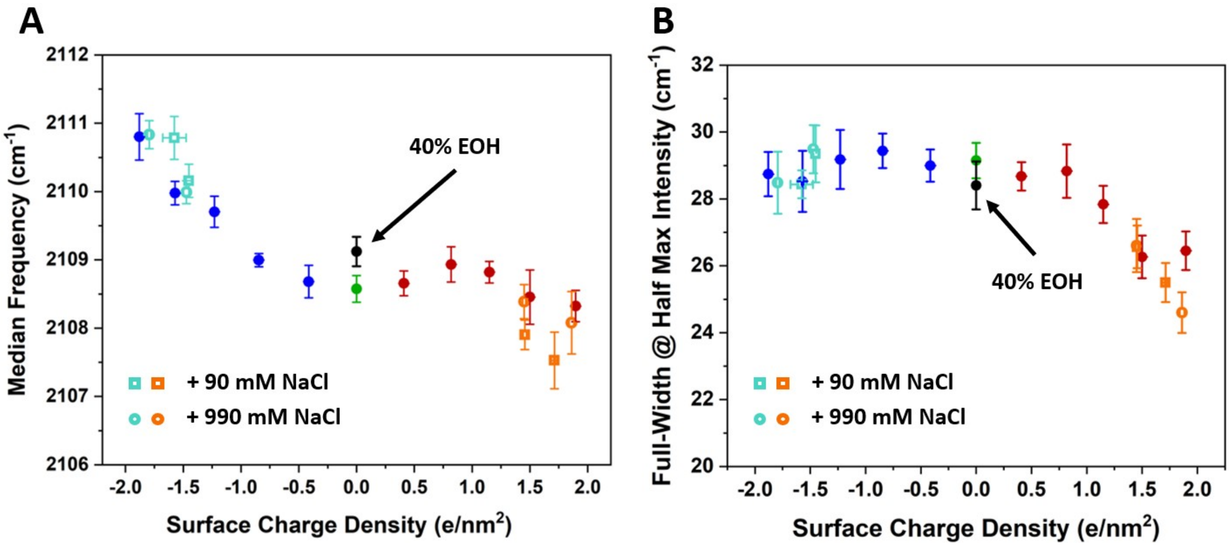

Fig. S29 (**A**) Azide peak median frequency (**Fig. S20A**) and (**B**) azide peak FWHM (**Fig. S20B)** including data points with added NaCl to the subphase and 40% EOH monolayers.

S7. Experimental Peak Properties - 9 Trials*

*6 trials for 30% ESO$_4^-$ over 10 mM NaOH (**Table S4**)

Table S3.100% AzEOH Monolayers

	10 mM NaOH	**10 mM HCl**	**Both**
Peak Area 2070-2170 cm^{-1}	0.049 (0.002)	0.049 (0.003)	0.049 (0.002)
Mode Frequency (cm^{-1})	2105.4 (0.2)	2105.5 (0.2)	2105.4 (0.2)
Med. Frequency (cm^{-1}) 2080-2140 cm^{-1}	2108.5 (0.2)	2108.6 (0.2)	2108.6 (0.2)
Med. Frequency (cm^{-1}) 2070-2170 cm^{-1}	2110.5 (0.7)	2109.8 (0.5)	2110.1 (0.7)
FWHM (cm^{-1})	29.3 (0.5)	29.0 (0.6)	29.1 (0.5)

Table S4 Mixed Monolayers Containing ESO$_4^-$ (Sulphate) over 10 mM NaOH

	10% ESO$_4^-$	**20% ESO$_4^-$**	**30% ESO$_4^-$**	**40% ESO$_4^-$**	**50% ESO$_4^-$**
Peak Area 2070-2170 cm^{-1}	0.044 (0.002)	0.040 (0.001)	0.032 (0.001)	0.026 (0.001)	0.023 (0.001)
Mode Frequency (cm^{-1})	2105.6 (0.1)	2106.1 (0.3)	2106.8 (0.4)	2107.8 (0.3)	2108.3 (0.5)
Med. Frequency (cm^{-1}) 2080-2140 cm^{-1}	2108.7 (0.2)	2109.0 (0.1)	2109.7 (0.2)	2110.0 (0.2)	2110.8 (0.3)
Med. Frequency (cm^{-1}) 2070-2170 cm^{-1}	2110.3 (0.5)	2111.0 (0.4)	2111.2 (0.5)	2111.5 (0.5)	2113.0 (1.0)
FWHM (cm^{-1})	29.0 (0.5)	29.4 (0.5)	29.2 (0.9)	28.5 (0.9)	28.7 (0.7)

Table S5 Mixed Monolayers Containing ENH$_3^+$ (Ammonium) over 10 mM HCl

	10% ENH$_3^+$	**20% ENH$_3^+$**	**30% ENH$_3^+$**	**40% ENH$_3^+$**	**50% ENH$_3^+$**
Peak Area 2070-2170 cm^{-1}	0.043 (0.002)	0.041 (0.002)	0.033 (0.002)	0.029 (0.001)	0.0238 (0.0009)
Mode Frequency (cm^{-1})	2105.8 (0.2)	2105.9 (0.3)	2106.2 (0.3)	2106.2 (0.3)	2106.1 (0.2)
Med. Frequency (cm^{-1}) 2080-2140 cm^{-1}	2108.7 (0.2)	2108.9 (0.3)	2108.8 (0.3)	2108.5 (0.4)	2108.3 (0.2)
Med. Frequency (cm^{-1}) 2070-2170 cm^{-1}	2110.2 (0.6)	2111.0 (0.8)	2110.5 (0.5)	2109.8 (0.8)	2110.1 (0.5)
FWHM (cm^{-1})	28.7 (0.4)	28.8 (0.8)	27.8 (0.6)	26.3 (0.6)	26.4 (0.6)

Table S6 Mixed Monolayers Containing ESO_4^- (Sulphate) over 10 mM NaOH + 90 mM NaCl

	40% ESO_4^-	**50% ESO_4^-**
Peak Area 2070-2170 cm^{-1}	0.029 (0.002)	0.022 (0.002)
Mode Frequency (cm^{-1})	2107.6 (0.4)	2108.7 (0.3)
Med. Frequency (cm^{-1}) 2080-2140 cm^{-1}	2110.0 (0.2)	2110.8 (0.2)
Med. Frequency (cm^{-1}) 2070-2170 cm^{-1}	2111.6 (0.9)	2112.8 (0.9)
FWHM (cm^{-1})	29.5 (0.7)	28.5 (0.9)

Table S7 Mixed Monolayers Containing ENH_3^+ (Ammonium) over 10 mM HCl + 90 mM NaCl

	40% ENH_3^+	**50% ENH_3^+**
Peak Area 2070-2170 cm^{-1}	0.030 (0.001)	0.021 (0.001)
Mode Frequency (cm^{-1})	2105.8 (0.4)	2106.2 (0.4)
Med. Frequency (cm^{-1}) 2080-2140 cm^{-1}	2108.4 (0.2)	2108.1 (0.5)
Med. Frequency (cm^{-1}) 2070-2170 cm^{-1}	2109.6 (0.3)	2109.2 (0.7)
FWHM (cm^{-1})	26.6 (0.8)	24.6 (0.6)

Table S8 Mixed Monolayers Containing ESO_4^- (Sulphate) over 10 mM NaOH + 990 mM NaCl

	40% ESO_4^-	**50% ESO_4^-**
Peak Area 2070-2170 cm^{-1}	0.026 (0.002)	0.021 (0.001)
Mode Frequency (cm^{-1})	2108.1 (0.4)	2108.6 (0.5)
Med. Frequency (cm^{-1}) 2080-2140 cm^{-1}	2110.2 (0.2)	2110.8 (0.3)
Med. Frequency (cm^{-1}) 2070-2170 cm^{-1}	2111.3 (1.2)	2112.9 (0.6)
FWHM (cm^{-1})	29.3 (0.9)	28.4 (0.4)

Table S9 Mixed Monolayers Containing ENH_3^+ (Ammonium) over 10 mM HCl + 990 mM NaCl

	40% ENH_3^+	**50% ENH_3^+**
Peak Area 2070-2170 cm^{-1}	0.029 (0.001)	0.022 (0.001)
Mode Frequency (cm^{-1})	2105.7 (0.3)	2105.3 (0.5)
Med. Frequency (cm^{-1}) 2080-2140 cm^{-1}	2107.9 (0.2)	2107.5 (0.4)
Med. Frequency (cm^{-1}) 2070-2170 cm^{-1}	2109.4 (0.5)	2108.6 (1.0)
FWHM (cm^{-1})	26.6 (0.6)	25.5 (0.6)

Table S10 40% EOH, 60% AzEOH Monolayers

	10 mM NaOH	**10 mM HCl**	**Both**
Peak Area 2070-2170 cm^{-1}	0.030 (0.001)	0.031 (0.001)	0.030 (0.001)
Mode Frequency (cm^{-1})	2106.5 (0.3)	2106.9 (0.4)	2106.7 (0.4)
Med. Frequency (cm^{-1}) 2080-2140 cm^{-1}	2109.0 (0.2)	2109.2 (0.2)	2109.1 (0.2)
Med. Frequency (cm^{-1}) 2070-2170 cm^{-1}	2110.3 (0.6)	2111.2 (0.7)	2110.7 (0.7)
FWHM (cm^{-1})	28.8 (0.6)	28.0 (0.6)	28.4 (0.7)

References

1 E. C. Griffith, E. M. Adams, H. C. Allen, V. Vaida, *J. Phys. Chem. B,* 2012, **116,** 7849–7857.

2 M. Shrestha, M.Luo, Y. Li, B. Xiang, W. Xiong, V. H. Grassian, *Chem. Sci.,* 2018, **9**, 5716–5723.

3 A. M. Deal, V. Vaida, *J. Phys. Chem. A,* 2022, **126**, 8280–8294.

4 A. J. Bard, L. R. Faulkner, H. S. White, *Electrochemical Methods: Fundamentals and Applications*; John Wiley & Sons, 2022.

5 M. P. Wolfshorndl, R. Baskin, I. Dhawan, C. H. Londergan, *J. Phys. Chem. B,* 2012, **116**, 1172–1179.